s-wave scattering lengths for the ^{7}Be + *p* system from an *R*-matrix analysis

S. N. Paneru,[1,*] C. R. Brune,[1] R. Giri,[1] R. J. Livesay,[2] U. Greife,[2] J. C. Blackmon,[3] D. W. Bardayan,[4] K. A. Chipps,[5] B. Davids,[6,7] D. S. Connolly,[6] K. Y. Chae,[8] A. E. Champagne,[9] C. Deibel,[10] K. L. Jones,[11,12] M. S. Johnson,[12] R. L. Kozub,[13] Z. Ma,[11] C. D. Nesaraja,[5,11] S. D. Pain,[12] F. Sarazin,[2] J. F. Shriner Jr.,[13] D. W. Stracener,[5] M. S. Smith,[5] J. S. Thomas,[12] D. W. Visser,[9] and C. Wrede[10]

[1]*Department of Physics and Astronomy, Ohio University, Athens, Ohio 45701, USA*
[2]*Department of Physics, Colorado School of Mines, Golden, Colorado 80401, USA*
[3]*Department of Physics and Astronomy, Louisiana State University, Baton Rouge, Louisiana 70803, USA*
[4]*Department of Physics, University of Notre Dame, Notre Dame, Indiana 46556, USA*
[5]*Physics Division, Oak Ridge National Laboratory, Oak Ridge, Tennessee 37831, USA*
[6]*TRIUMF, Vancouver, British Columbia V6T 2A3, Canada*
[7]*Physics Department, Simon Fraser University, Burnaby, British Columbia V5A 1S6, Canada*
[8]*Department of Physics, Sungkyunkwan University, Suwon 16419, Korea*
[9]*Department of Physics and Astronomy, University of North Carolina, Chapel Hill, North Carolina 27599, USA*
[10]*Wright Nuclear Structure Laboratory, Yale University, New Haven, Connecticut 06520, USA*
[11]*Department of Physics and Astronomy, University of Tennessee, Knoxville, Tennessee 37996, USA*
[12]*Department of Physics and Astronomy, Rutgers University, Piscataway, New Jersey 08854, USA*
[13]*Physics Department, Tennessee Technological University, Cookeville, Tennessee 38505, USA*

(Received 4 February 2019; published 30 April 2019)

The astrophysical *S* factor for the radiative proton capture reaction on ^{7}Be (S_{17}) at low energies is affected by the *s*-wave scattering lengths. We report the measurement of elastic and inelastic scattering cross sections for the ^{7}Be + *p* system in the center-of-mass energy range 0.474–2.740 MeV and center-of-mass angular range 70°–150°. A radioactive ^{7}Be beam produced at Oak Ridge National Laboratory's (ORNL) Holifield Radioactive Ion Beam Facility was accelerated and bombarded a thin polypropylene $(CH_2)_n$ target. Scattered ions were detected in the segmented Silicon Detector Array. Using an *R*-matrix analysis of ORNL and Louvain-la-Neuve cross-section data, the *s*-wave scattering lengths for channel spins 1 and 2 were determined to be $17.34^{+1.11}_{-1.33}$ and $-3.18^{+0.55}_{-0.50}$ fm, respectively. The uncertainty in the *s*-wave scattering lengths reported in this work is smaller by a factor of 5–8 compared to the previous measurement, which may reduce the overall uncertainty in S_{17} at zero energy. The level structure of ^{8}B is discussed based upon the results from this work. Evidence for the existence of 0^+ and 2^+ levels in ^{8}B at 1.9 and 2.21 MeV, respectively, is observed.

DOI: 10.1103/PhysRevC.99.045807

I. INTRODUCTION

The total terrestrial flux of high-energy neutrinos resulting from the β^+ decay of ^{8}B in the Sun has been measured with a precision of ±4% [1,2]. Comparisons of the measured and predicted ^{8}B solar neutrino fluxes are therefore limited primarily by the theoretical uncertainty of approximately ±14% associated with standard solar model predictions [3]. The low-energy astrophysical *S* factor for the ^{7}Be$(p,\gamma)^8$B radiative capture reaction, $S_{17}(E)$, is the most uncertain nuclear input needed to predict the ^{8}B solar neutrino flux [4,5] in the standard solar model. It must be known at or near the Gamow peak of ∼18 keV, which is experimentally inaccessible due to the Coulomb barrier [6]. The cross sections are unmeasurably small at these energies, so available data starting around 100 keV above the Gamow peak must be extrapolated to solar energies with the aid of theoretical models.

Descouvemont [7] used a microscopic three-cluster model and a potential model to study the theoretical uncertainty in extrapolating S_{17} to zero energy and found that below 1 MeV it is dominated by the uncertainties in the *s*-wave scattering lengths for the ^{7}Be + *p* system. A leading-order calculation of ^{7}Be$(p,\gamma)^8$B in a low-energy effective field theory [8] found that the experimental uncertainties in the scattering lengths strongly affected the calculation at energies as low as 400 keV. A simple potential model [9] shows the importance of the *s*-wave scattering lengths in extrapolating S_{17} to zero energy, although it is not clear how the results in this paper can be translated into uncertainties in the $S_{17}(0)$ value deduced from capture data. Although one recent effective field theory calculation [10] suggests that the contribution of scattering length uncertainties to the extrapolation uncertainty of S_{17} below 500 keV may not be large, this sensitivity depends on the range of scattering lengths considered in the calculation.

Owing to the required use of radioactive ^{7}Be (half-life = 53.2 days), the scattering lengths have only been measured once, by Angulo *et al.* [11], who found $a_{01} = 25 \pm 9$ fm and

*sp266413@ohio.edu

$a_{02} = -7 \pm 3$ fm, where a_{0I} is the s-wave scattering length for channel spin I. The s-wave scattering lengths deduced from the *ab initio* no-core shell model/resonating group method [12] are $a_{01} = -5.2$ fm and $a_{02} = -15.3$ fm. Discrepancies in the predicted and measured s-wave scattering lengths, particularly for channel spin 2, demand caution when using theoretical models in the extrapolation of S_{17} to zero energy. Reference [12] also calculates the astrophysical S factor for ^{7}Be$(p,\gamma)^8$B radiative capture reaction at zero energy, but the relationship between the s-wave scattering lengths and $S_{17}(0)$ is not highlighted. Better constraints on the scattering lengths may lead to a significant reduction in the uncertainty of $S_{17}(0)$, thereby reducing the overall uncertainty in the ^{8}B neutrino flux prediction.

The evaluation of S_{17} in the energy range below 100 keV depends on complete knowledge of the low-lying energy levels of ^{8}B, which remains elusive [13]. There have been several ^{7}Be + p elastic scattering measurements aimed at elucidating the level structure of ^{8}B. Gol'dberg *et al.* [14] measured the elastic scattering excitation function with a thick target at relative kinetic energies E from 1 to 3.6 MeV at 0° in inverse kinematics and proposed the existence of a 1^+ level at $E_x = 2.83$ MeV with a width of 780 keV. Rogachev *et al.* [15] measured elastic scattering using a thick target over a relative kinetic energy range from 1 to 3.3 MeV and found evidence for the existence of a 2^- level at $E_x = 3.5 \pm 0.5$ MeV with a width of 8 ± 4 MeV. Angulo *et al.* [11] measured the ^{7}Be + p elastic cross section with a thin polyethylene target from $E =$ 0.3 MeV to $E = 0.75$ MeV. From an R-matrix analysis, the scattering lengths were inferred and the width of the 1^+ resonance at $E = 634 \pm 5$ keV was determined to be 31 ± 4 keV. Yamaguchi *et al.* [16] measured resonant elastic and inelastic scattering from $E = 1.3$ to 6.7 MeV, adducing evidence for 2^- and 1^- states. Based on an R-matrix analysis of a recent thick-target elastic and inelastic scattering measurement, Mitchell *et al.* [17] proposed new low-lying 0^+, 2^+, and 1^+states at $E_x = 1.9$, 2.54, and 3.3 MeV, respectively, in ^{8}B. These levels have not yet been confirmed by further experiments. Thus far there has been only a single measurement of elastic scattering below $E = 1$ MeV and the available data at higher energies are inconsistent. Based on these experiments there are only two well-known excited states of ^{8}B, the 1^+ and 3^+ states at 0.77 and 2.32 MeV, respectively. All other states inferred on the basis of previous ^{7}Be + p elastic scattering measurements require further experimental verification.

This paper describes a new measurement of the elastic and inelastic scattering cross sections of ^{7}Be + p and a determination of the s-wave scattering lengths using an R-matrix analysis. It also presents evidence for the existence of various excited states in ^{8}B that must be properly described in theoretical models of its structure. The measurement of elastic and inelastic scattering was performed in inverse kinematics from $E_{\text{c.m.}} = 0.474$ MeV to $E_{\text{c.m.}} = 2.740$ MeV covering a center-of-mass angular range of 70° to 150°. We used the R-matrix method [18] to analyze elastic and inelastic scattering data. In this work, we confirm the existence of some of the levels reported in the literature and reassess that of others. In particular, we find no evidence in our data set for the 1^+ level at 3.3 MeV that has been reported in Ref. [17].

The experimental method used to measure the elastic and inelastic scattering is explained in Sec. II. We used a multichannel, multilevel R-matrix approach to analyze elastic and inelastic scattering data simultaneously. The best-fit parameters from the R-matrix analysis were used to determine the s-wave scattering lengths using the method described in Sec. III. Section IV contains the findings of this work and a comparison with available data from the literature. We conclude in Sec. V.

II. EXPERIMENT

The elastic and inelastic ^{7}Be + p scattering cross sections were measured in inverse kinematics between 0.474 and 2.740 MeV in the center-of-mass system at the Holifield Radioactive Ion Beam Facility (HRIBF) [19] of Oak Ridge National Laboratory (ORNL). ^{7}Be was produced at the Triangle University Nuclear Laboratory using the ^{7}Li$(p,n)^7$Be reaction [20]. The lithium targets (disks of 2-cm diameter and 3-mm thickness) were bombarded with 8- to 11-MeV protons, typically producing 240 mCi of ^{7}Be. The activity was transported to ORNL in the form of an ingot for chemical extraction and concentration using the method described in Ref. [21]. ^{7}Be ions were injected into the HRIBF's tandem accelerator via a cesium sputter source. The beam was stripped to the 4^+ charge state before the analyzing magnet, removing any ^{7}Li whose maximum charge state is 3^+. The fully stripped ^{7}Be beam was then directed into the target chamber hosting the Silicon Detector Array (SIDAR) [22]. Additional details of the experimental setup are provided in Ref. [23]. The SIDAR consists of an array of Micron YY1 detectors with 40-keV energy resolution, which can be arranged in either a lamp-shade (with six wedges) or a flat configuration (with eight wedges). We utilized the SIDAR in the flat configuration for this experiment. The array was composed of detectors of either 300- or 500-μm nominal thickness. A schematic diagram of the target station is shown in Fig. 1. Self-supporting thin foils of polypropylene $(CH_2)_n$ and gold (Au) were used as the targets. The thickness of the $(CH_2)_n$ target was determined via α-particle energy loss measurements to be 100 μg/cm^2, with an uncertainty of ±10% resulting from the stopping power calculations. The target foils were mounted on a retractable target ladder placed in the scattering chamber. There were two diagnostic tools on the ladder, namely, an aperture and a phosphor screen, which provide information about the location and size of the beam in the scattering chamber. The scattered protons were detected in the SIDAR located downstream of the target. The ionization chamber was separated from the target chamber by a 0.9-μm-thick mylar window and filled with 40 T of isobutane gas. The ionization chamber was used for tuning and beam diagnostics. The unscattered beam was blocked by a 1.5-cm aluminum disk that was small enough to let the scattered ^{7}Be ions enter into the ionization chamber.

The experiment was performed in two campaigns, for which the experimental configurations were similar. The measurements were taken using two different distances of the SIDAR from the target, providing overlapping angular ranges of $\theta_{\text{lab}} = 26°$–$50°$ and $\theta_{\text{lab}} = 14°$–$31°$. The ^{7}Be bombarding energies were chosen in 16 energy steps between 4 and

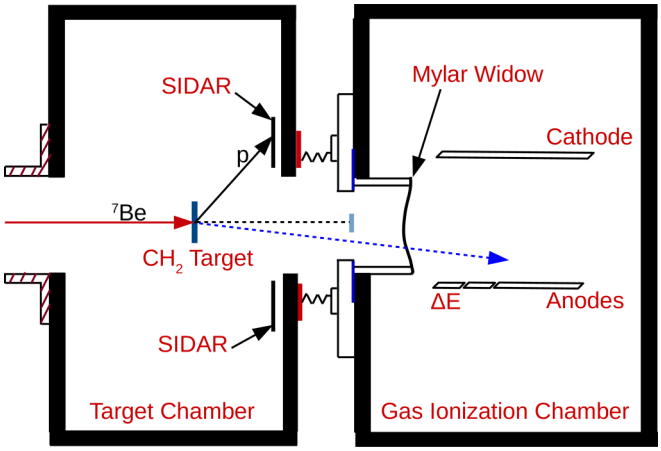

FIG. 1. Experimental setup [22]. The ^{7}Be beam delivered by HRIBF (on left) bombarded a thin polypropylene $(CH_2)_n$ target. Protons were detected by a SIDAR, which was mounted on the downstream face of the scattering chamber. The ion chamber placed downstream of the scattering chamber was used for tuning and beam diagnostics.

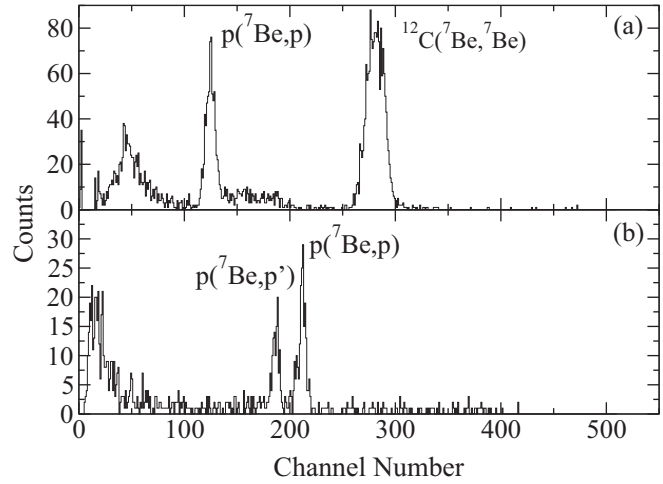

FIG. 2. Two spectra from the experiment. (a) Spectrum obtained with a $(CH_2)_n$ target at a ^{7}Be beam energy of 5.2 MeV and $\theta_{lab} = 37.4°$, where inelastic scattering events were not observed. (b) Spectrum obtained with a $(CH_2)_n$ target at a ^{7}Be beam energy of 20 MeV and $\theta_{lab} = 29.7°$, where proton elastic scattering events are well separated from proton inelastic scattering events. ^{7}Be + ^{12}C scattering events are not visible here because the gains were set to place the proton scattering data in the middle of the ADC range such that ^{7}Be + ^{12}C scattering events were beyond the range of ADC.

27 MeV with intensities of 10^6–10^7 pps at the target station. The ^{7}Be + p scattering cross sections were measured relative to the ^{7}Be+Au and ^{7}Be + ^{12}C scattering cross sections, which were used for normalization of the data. The energy loss in the target was taken into account by calculating the effective beam energy as $E_{eff} = E_0 - \Delta E/2$, where E_0 is the incident beam energy and ΔE is the energy loss in the target calculated using SRIM [24]. This procedure is valid as long as there is no strong energy dependence of the cross section over the energy range covered in the target. Since there is a resonance at $E_{c.m.} = 0.634$ MeV, the correction factors for the low-energy experimental data points were calculated using Eqs. (6) and (7) from Ref. [25]. The correction factor calculated for the 5.2-MeV measurement in the laboratory system was 0.90, while for all other experimental data points, the correction factor was within 2% of unity. This correction factor has been included in the analysis of the $E_{lab} = 5.2$ MeV measurement.

For each beam energy, there were two runs, for the purpose of separately collecting ^{7}Be + p and ^{7}Be + Au events. The two runs were performed with a $(CH_2)_n$ target and a combined target [i.e., a $(CH_2)_n$ foil with a Au foil in the back], respectively. The proton scattering events could be distinguished from the ^{7}Be + ^{12}C scattering events based upon their energies as shown in Fig. 2(a). Proton inelastic scattering events were only observed at high ^{7}Be beam energies. The proton inelastic scattering events were well separated from the proton elastic scattering events as shown in Fig. 2(b).

The ^{7}Be + p scattering data were normalized to simultaneous scattering reactions. The low-energy scattering data (for ^{7}Be beam energies of $E_{lab} = 4$, 4.5, and 5.2 MeV) were normalized to the ^{7}Be + ^{12}C scattering data, as the carbon scattering at these energies is well described by Rutherford scattering. At higher energies, the ^{7}Be + ^{12}C scattering starts deviating from Rutherford scattering as shown in Fig. 3. For ^{7}Be beam energies of $E_{lab} = 7$, 8, 9, 10, 11, 12, 13, and 16 MeV, the ^{7}Be + p scattering data were normalized to ^{7}Be + ^{12}C scattering cross sections, which were themselves normalized by ^{7}Be+Au scattering data. To utilize this normalization procedure, we need to know the carbon-to-gold ratio rather than the absolute target thickness assuming H/C = 2. The carbon-to-gold ratio was determined using the ratio of differential cross sections of ^{7}Be + ^{12}C and ^{7}Be + Au scattering, both of which are described by Rutherford scattering at small angles. The carbon-to-gold ratio was determined to be C/Au = 10.2 ± 0.7, where the quoted uncertainty is

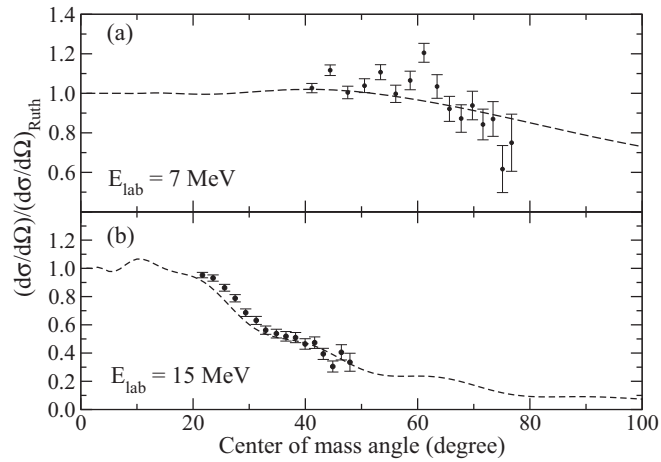

FIG. 3. ^{7}Be + ^{12}C scattering data from the experiment. (a) ^{7}Be + ^{12}C scattering data for a ^{7}Be beam energy of 7.0 MeV. (b) ^{7}Be + ^{12}C scattering data for a ^{7}Be beam energy of 15.0 MeV. Dashed curves are optical model calculations using the parameters from Ref. [26]

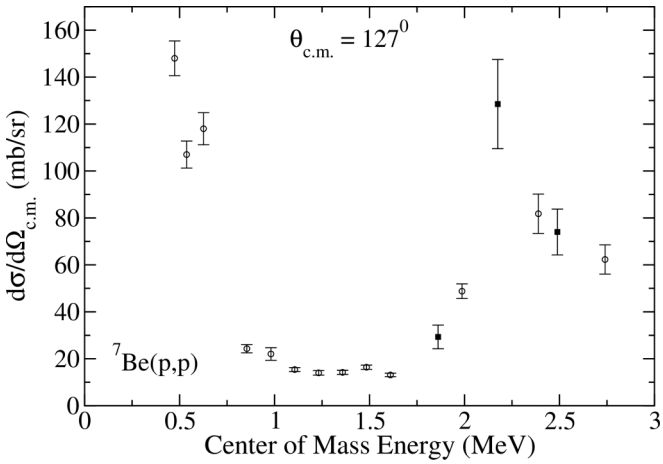

FIG. 4. Excitation function for $^7\mathrm{Be} + p$ elastic scattering at $\theta_{\mathrm{c.m.}} = 127^\circ$. Circles and squares correspond to the data from the first and second experimental campaigns, respectively.

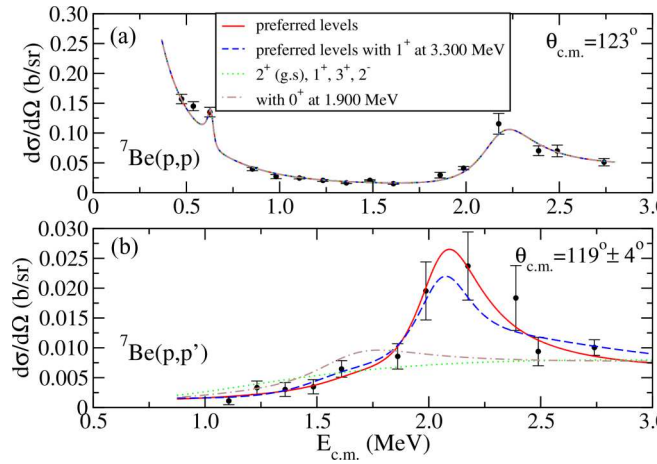

FIG. 5. *R*-matrix fit of elastic and inelastic scattering data from this work. The dotted green curve corresponds to the fit obtained with 2^+, 1^+, 3^+, and 2^- levels at 0, 0.77, 2.32, and 3.52 MeV, respectively. The dashed-dotted brown curve corresponds to the fit obtained with an additional 0^+ level at 1.9 MeV. The dashed blue curve corresponds to the fit with the preferred levels with an additional 1^+ level at 3.3 MeV and the solid red curve corresponds to the fit with the preferred levels only.

statistical in nature. For ^{7}Be beam energies of $E_{\mathrm{lab}} = 19.2$ and 22 MeV, the proton scattering data were normalized directly to the $^7\mathrm{Be} + \mathrm{Au}$ scattering data, as $^7\mathrm{Be} + \mathrm{Au}$ scattering at all angles and energies covered in this experiment is well described by Rutherford scattering. For three beam energies ($E_{\mathrm{lab}} =$ 15, 17.5, and 20 MeV), $^7\mathrm{Be} + \mathrm{Au}$ scattering was not measured and $^7\mathrm{Be} + {}^{12}\mathrm{C}$ cross sections were not experimentally determined. For these energies the $^7\mathrm{Be} + p$ scattering was normalized to the $^7\mathrm{Be} + {}^{12}\mathrm{C}$ elastic scattering cross section calculated via the optical model using the DWUCK5 code [27]. The $^7\mathrm{Li} + {}^{12}\mathrm{C}$ optical model parameters from Ref. [28] were used to describe $^7\mathrm{Be} + {}^{12}\mathrm{C}$ elastic scattering by changing the charge and the incident energy. This parametrization was found to give a good agreement, to within 10% of the $^7\mathrm{Be} + {}^{12}\mathrm{C}$ elastic scattering data at energies where the normalization was determined independently.

The normalization procedures explained before depend on the ratio of the target atoms. The hydrogen-to-carbon ratio in the target was determined from the 4-MeV ^{7}Be measurement using the ratio of $^7\mathrm{Be} + p$ and $^7\mathrm{Be} + {}^{12}\mathrm{C}$ scattering, both of which were assumed to be Rutherford scattering. The systematic uncertainty for ^{7}Be measurements of $E_{\mathrm{lab}} = 4$, 4.5, 5.2, 15, 17.5, and 20 MeV, which depends on the hydrogen-to-carbon ratio, was estimated to be $\pm 6\%$. For ^{7}Be beam energies of $E_{\mathrm{lab}} = 7$, 8, 9, 10, 11, 12, 13, and 16 MeV, the normalization procedure depends on the carbon-to-gold ratio, and the systematic uncertainty was estimated to be $\pm 6\%$. For measurements at $E_{\mathrm{lab}} = 19.2$ and 22 MeV, the normalization procedure depends on the hydrogen-to-gold ratio, and the systematic uncertainty was estimated to be $\pm 7\%$. The optical model analysis used for three beam energies ($E_{\mathrm{lab}} = 15$, 17.5, and 20 MeV) has an additional systematic uncertainty of $\pm 7\%$, thus the overall systematic uncertainty for these energies was estimated to be $\pm 10\%$.

Figure 4 shows the excitation function for elastic scattering of $^7\mathrm{Be} + p$ measured in this work. Circles and squares correspond to the data from the first and second experimental campaigns, respectively.

III. *R*-MATRIX ANALYSIS

The differential scattering cross section for $^7\mathrm{Be}(p, p)^7\mathrm{Be}$ is described using *R*-matrix theory [18]. The elastic and inelastic cross-section data from this experiment and low-energy elastic scattering data from Angulo *et al.* [11] have been analyzed using the multilevel multichannel code AZURE2 [29]. The alternative parametrization of the *R*-matrix theory presented in Ref. [30] is used. So, the *R* matrix can be expressed in terms of alternative parameters, namely, the observed resonance energy $\tilde{E}$ and the observed reduced width amplitude $\tilde{\gamma}$. A channel radius of 4.3 fm is assumed and the background poles have been fixed at particular excitation energies.

The spins of the ground and first excited states of ^{7}Be are $3/2^-$ and $1/2^-$, respectively. If we restrict our calculations up to *p* waves, then the allowed levels in ^{8}B following the coupling scheme would be 0^-, 0^+, 1^-, 1^+, 2^-, 2^+, and 3^+. The *R*-matrix analysis was started with the states of ^{8}B identified in previous experiments [11,14–17], namely, the 2^+, 1^+, 3^+, and 2^- levels at excitation energies of 0, 0.77, 2.32, and 3.52 MeV, respectively. The separation energies for the levels introduced in the *R*-matrix analysis were taken from Ref. [31]. The values of the asymptotic normalization constants (ANCs) used for the ground state in this analysis are $C^2_{(^3P_2)} = 0.0990(57)$ fm^{-1}, $C^2_{(^5P_2)} = 0.438(23)$ fm^{-1}, and $C^2_{(^3P_2^*)} = 0.1215(36)$ fm^{-1} [32], where the third value refers to the ^{7}Be excited-state component and the ANCs were obtained using *ab initio* methods [33]. The fit to the scattering data is not highly sensitive to the choice of ANC values in this analysis. These states reproduce the fits to the elastic scattering data reasonably well, as shown in Fig. 5, but could not explain the inelastic scattering data. In Fig. 5(b), data points correspond to the inelastic scattering cross section for a center-of-mass angle $119^\circ \pm 4^\circ$. The conversion from

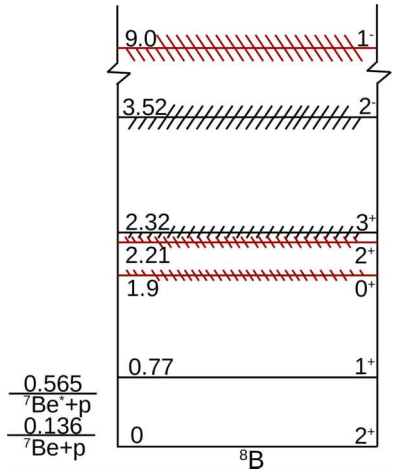

FIG. 6. Level structure for ^{8}B. This work supports the existence of states shown in red that have been previously suggested in Ref. [17].

laboratory angle to center-of-mass angle was done taking into account the correct kinematics for inelastic scattering. Under the assumption of just the known literature values the inelastic channel was not well reproduced, so alternative level schemes were used for the R-matrix parameters in order to improve the fit. Additional 0^+, 1^-, and 2^+ states at excitation energies of 1.9, 9.0, and 2.21 MeV were introduced to improve the fits to the inelastic scattering data with no significant changes in the fits to the elastic scattering data. The 0^+ level at an excitation energy of 1.9 MeV in ^{8}B was previously suggested in Ref. [17]. The 1^- level is introduced as a background level in our fits. In the phenomenological R-matrix theory, levels introduced at energies higher than the highest energy data points and with large widths are termed background levels. The solid red line in Fig. 5 represents the fit with all these levels. These levels are defined as preferred levels hereafter. It can be infered from Fig. 5 that the 2^+ level at 2.21 MeV is required to fit the inelastic scattering data well. The introduction of an additional 2^- level at 9.0 MeV as a background level does not change significantly the fits to the data, so it was not included in our final fit. The sensitivity of the fit to the excitation energy of the 2^+ level was studied and we differ in the extracted excitation energy for such a level from Ref. [17].

The existence of a 1^+ level around 2 to 3 MeV in ^{8}B has often been questioned. Gol'dberg *et al.* [14] suggested a 1^+ level at 2.83 ± 0.150 MeV with a width of 780 ± 200 keV. Mitchell *et al.* [17] introduced a 1^+ level at 3.3 MeV with a width of 2.8 MeV. The recoil-corrected continuum shell-model calculations in Ref. [34] also suggested the presence of a 1^+ level in ^{8}B requiring verification by inelastic scattering measurements. The dashed blue curve in Fig. 5 shows the effect of a 1^+ level at an excitation energy of 3.3 MeV along with the preferred levels. The fits to the data with and without this 1^+ level can be compared in Fig. 5. There is no significant change in the elastic excitation function but the inelastic scattering cross section is underestimated. Therefore, based on the scattering data available for ^{7}Be + p, there is no conclusive evidence for a 1^+ level at an excitation energy of 3.3 MeV. Based on the analysis of these data, the level structure of the ^{8}B is shown in Fig. 6.

TABLE I. Normalization factors, χ^2, and number of data points (N) for angular distributions of the ORNL measurement (parts A and B) and excitation function from Ref. [11] (part C). The energies and the angles are in the center-of-mass frame.

Reaction ($E_{\text{c.m.}}/\theta_{\text{c.m.}}$)	Norm	χ^2	N
	(A) ^{7}Be(p, p)^{7}Be		
0.474 MeV	1.012	37.750	16
0.537 MeV	1.283	53.301	16
0.626 MeV	1.039	17.119	16
0.854 MeV	1.274	24.176	16
0.981 MeV	1.375	3.333	4
1.106 MeV	1.300	18.982	16
1.232 MeV	1.177	12.599	16
1.358 MeV	1.144	8.223	16
1.484 MeV	1.039	29.985	16
1.610 MeV	1.032	14.725	16
1.861 MeV	0.893	10.891	12
1.987 MeV	0.781	15.205	16
2.175 MeV	0.964	5.815	13
2.389 MeV	0.987	6.270	16
2.489 MeV	0.933	2.706	13
2.740 MeV	0.908	3.351	16
	(B) ^{7}Be(p, p')^{7}Be($1/2^-$)		
1.106 MeV	1.060	27.143	11
1.232 MeV	1.177	34.612	14
1.358 MeV	1.022	6.982	12
1.484 MeV	0.871	13.540	15
1.610 MeV	0.858	21.685	12
1.861 MeV	1.398	20.647	16
1.987 MeV	0.939	5.095	16
2.175 MeV	0.980	2.020	6
2.389 MeV	1.120	12.803	16
2.489 MeV	0.930	13.521	10
2.740 MeV	0.713	46.574	16
	(C) ^{7}Be(p, p)^{7}Be		
120.24°–131.13°	0.987	98.966	87
156.62°–170.21°	0.978	236.707	343

Scattering length from R-matrix analysis

In this section, we relate the s-wave scattering lengths to the best-fit R-matrix parameters. The collision matrix $U_{c'c}$ can be expressed as

$$U_{c'c} = \Omega_{c'}\Omega_c[\delta_{c'c} + 2i(P_{c'}P_c)^{1/2}M_{c'c}], \quad (1)$$

where $M_{c'c} = \tilde{\gamma}_{c'}^T \tilde{\mathbf{A}} \tilde{\gamma}_c$. $\tilde{\mathbf{A}}$ is the level matrix as defined in Ref. [30], P_c is the penetration factor, and c is the channel index. For single-channel elastic scattering Eq. (1) reduces to

$$U_{cc} = \Omega_c^2[1 + 2iP_c(E)M_{cc}], \quad (2)$$

where

$$\Omega_c = e^{i(\omega_c - \phi_c)}. \quad (3)$$

TABLE II. Observed energies and reduced width amplitudes obtained from the best R matrix fit with the channel radius set at 4.3 fm. States with excitation energy in the parentheses are introduced as background levels. Parameter values in boldface were treated as fit parameters and all others were held constant. The observed partial widths can be computed from the reduced width amplitudes using Eq. (41) of Ref. [29].

J^π	$\tilde{E}_x$ (MeV)	$\tilde{\gamma}_{\rm el}$ $S=1$ (MeV$^{\frac{1}{2}}$)	$\tilde{\gamma}_{\rm el}$ $S=2$ (MeV$^{\frac{1}{2}}$)	$\tilde{\gamma}_{\rm inl}$ $S=0$ (MeV$^{\frac{1}{2}}$)	$\tilde{\gamma}_{\rm inl}$ $S=1$ (MeV$^{\frac{1}{2}}$)
2^+	0.000	−0.456	−0.959	0.000	0.510
1^+	0.774	**1.484**	**−0.268**	**−0.004**	**2.904**
0^+	1.900	**0.501**	0.000	0.000	**1.201**
2^+	2.210	**−0.274**	**0.323**	0.000	**0.632**
3^+	2.320	0.000	0.607	0.000	0.000
2^-	3.520	0.000	**1.700**	0.000	0.000
1^-	(9.000)	**1.433**	0.000	0.000	**−1.822**
2^+	(9.000)	**−77.322**	**−332.657**	0.000	**66.565**
3^+	(14.000)	0.000	**1.514**	0.000	0.000

The quantities ϕ_c and ω_c are the hard-sphere phase shift and Coulomb phase shift, respectively. For s-wave scattering ($l = 0$), $\omega_c = 0$. For diagonal collision matrix elements, $U_{cc} = e^{2i\delta_c}$, where δ_c is the total phase shift. In this case, the phase shift can be related to R-matrix parameters via

$$e^{2i\delta_c} = e^{-2i\phi_c}[1 + 2iP_c(E)M_{cc}]. \tag{4}$$

In the low-energy limit, Eq. (4) can be written as

$$\lim_{k\to 0} \cot\delta_0 = \frac{1}{-\phi_0 + P_0 M_{cc}}, \tag{5}$$

with $P_0 = ka/G_0^2(ka)$; a is the channel radius, k is the wave number, and G_0 is the irregular Coulomb function for $l = 0$. In the limit $k \to 0$, the effective range expansion from [35] can be reduced to

$$\lim_{k\to 0}\left[kC_0^2 \cot\delta_0\right] = -\frac{1}{a_0}, \tag{6}$$

where $C_0^2 = 2\pi\eta/(e^{2\pi\eta} - 1)$, with η the Sommerfeld parameter. From Eq. (5) and Eq. (6), the expression for the s-wave scattering length (a_0) in terms of R-matrix parameters is obtained as

$$a_0 = -a\left[\frac{M_{cc}}{x^2K_1^2(x)} - \frac{2I_1(x)}{x^2K_1(x)}\right], \tag{7}$$

where $I_1(x)$ and $K_1(x)$ are modified Bessel functions and $x = (8Z_1Z_2e^2\mu a/\hbar^2)^{1/2}$, Z_1e and Z_2e are the nuclear charges, $\hbar$ is the reduced Planck's constant, μ is the reduced mass, and a is the R-matrix channel radius. The Coulomb functions have been expressed in terms of modified Bessel functions using Ref. [36].

IV. RESULTS

The elastic and inelastic angular distribution data from the ORNL measurement and the elastic scattering data from Ref. [11] have been fitted simultaneously. The low-energy data from Ref. [11] were introduced to constrain the fits below

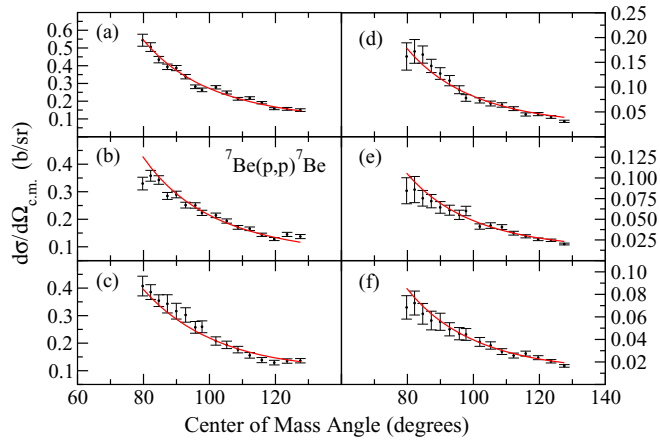

FIG. 7. Fits to the ^{7}Be$(p, p)^7$Be angular distribution data from this work at (a) $E_{\rm c.m.} = 0.474$ MeV, (b) $E_{\rm c.m.} = 0.537$ MeV, (c) $E_{\rm c.m.} = 0.626$ MeV, (d) $E_{\rm c.m.} = 0.854$ MeV, (e) $E_{\rm c.m.} = 1.106$ MeV, and (f) $E_{\rm c.m.} = 1.232$ MeV.

1-MeV center-of-mass energy. The systematic uncertainties of both data sets were introduced in the simultaneous fitting. In AZURE2, the systematic uncertainty for the data is introduced in the normalization of the data. A systematic uncertainty of ±5.5% has been assumed for the data from Ref. [11] as quoted in the paper, while the systematic uncertainties for different angular distributions from the ORNL measurement are included as explained in Sec. II. The absolute normalization of the data is allowed to vary during the fits. The output of the fit along with the chi-square values for each data segment are presented in Table I. The best-fit parameters from the simultaneous fitting are presented in Table II.

The fits to the elastic angular distributions are presented in Figs. 7, 8, and 9 and the fits to the inelastic angular distributions are presented in Fig. 10 and Fig. 11. The fits to data from Ref. [11] are shown in Fig. 12.

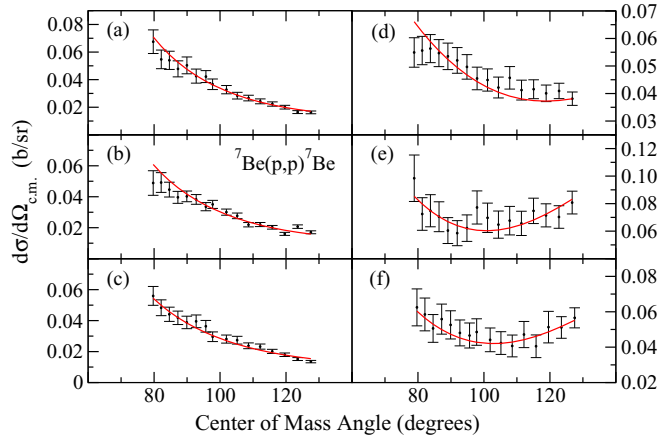

FIG. 8. Fits to the ^{7}Be$(p, p)^7$Be angular distribution data from this work at (a) $E_{\rm c.m.} = 1.358$ MeV, (b) $E_{\rm c.m.} = 1.484$ MeV, (c) $E_{\rm c.m.} = 1.610$ MeV, (d) $E_{\rm c.m.} = 1.987$ MeV, (e) $E_{\rm c.m.} = 2.389$ MeV, and (f) $E_{\rm c.m.} = 2.740$ MeV.

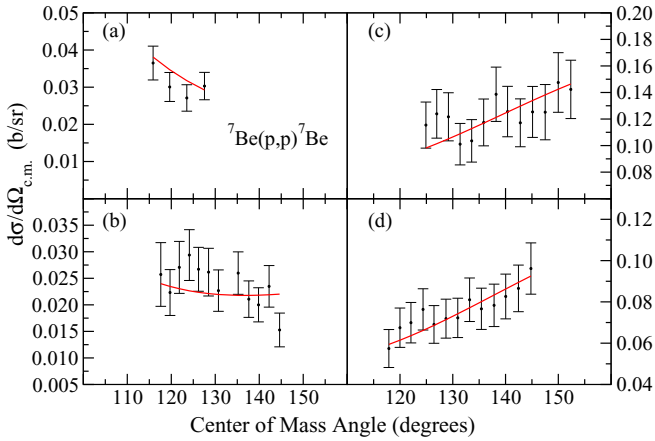

FIG. 9. Fits to the ^{7}Be(p, p)^{7}Be angular distribution data from this work at (a) $E_{c.m.} = 0.981$ MeV, (b) $E_{c.m.} = 1.861$ MeV, (c) $E_{c.m.} = 2.175$ MeV, and (d) $E_{c.m.} = 2.489$ MeV.

Using the best-fit parameters from Table II and Eq. (7), the s-wave scattering lengths for channel spins 1 and 2 were calculated to be $17.34^{+1.11}_{-1.33}$ and $-3.18^{+0.55}_{-0.50}$ fm, respectively. To illustrate the sensitivity of the fit to the reduced width amplitudes of the 1^- and 2^- levels, the reduced width amplitudes for these levels were varied and the changes in the total χ^2 were compared. A change of $\Delta\chi^2 = 1$ is used to define the acceptable range of the reduced width amplitudes for these levels, which gives the error bars in the scattering length values for channel spins 1 and 2, respectively. Using the same approach, the 1σ error bar was estimated for the parameters of the 0^+ and 2^+ levels. The widths of the 0^+ level are $\Gamma_p = 0.120 \pm 0.028$ MeV and $\Gamma_{p'} = 0.428 \pm 0.130$ MeV, where Γ_p and $\Gamma_{p'}$ refer to the elastic and inelastic channel widths, respectively. Similarly, the widths of the 2^+ level are $\Gamma_p = 0.024 \pm 0.009$ MeV and $\Gamma_{p'} = 0.230 \pm 0.001$ MeV. The excitation energies of the 0^+ and 2^+ levels are 1.9 ± 0.1 and 2.21 ± 0.04 MeV, respectively. Our excitation energy for the 2^+ level differs from the value presented in Ref. [17].

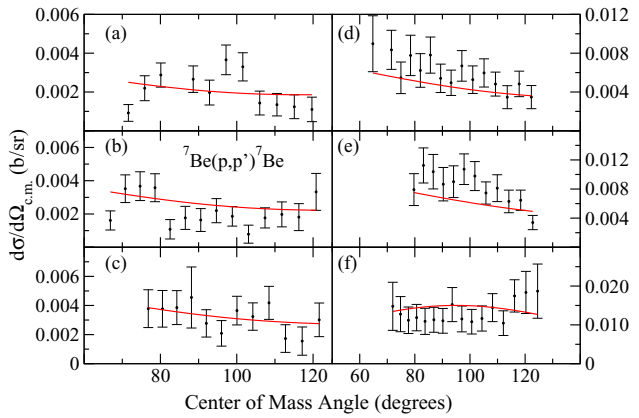

FIG. 10. Fits to the ^{7}Be(p, p')^{7}Be angular distribution data from this work at (a) $E_{c.m.} = 1.106$ MeV, (b) $E_{c.m.} = 1.232$ MeV, (c) $E_{c.m.} = 1.358$ MeV, (d) $E_{c.m.} = 1.484$ MeV, (e) $E_{c.m.} = 1.610$ MeV, and (f) $E_{c.m.} = 2.389$ MeV.

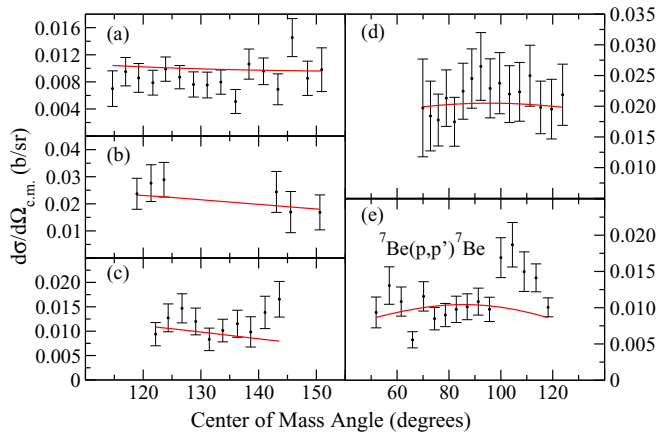

FIG. 11. Fits to the ^{7}Be(p, p')^{7}Be angular distribution data from this work at (a) $E_{c.m.} = 1.861$ MeV, (b) $E_{c.m.} = 2.175$ MeV, (c) $E_{c.m.} = 2.489$ MeV, (d) $E_{c.m.} = 1.987$ MeV, and (e) $E_{c.m.} = 2.74$ MeV.

The elastic proton partial width for the 1^+ state (0.77 MeV) from our analysis is in agreement with the value reported in Ref. [11].

Table I lists the χ^2 values of the fit to each data set. The fits to the first two data segments in both the elastic and the inelastic scattering from this work have a large χ^2. There are no obvious reasons for this, but point-to-point uncertainty is one possible explanation. Sensitivity tests were performed by excluding segments with large χ^2 values (i.e., $\chi^2/N > 2$) and segments with normalization factors above or below 20% (i.e., Norm < 0.80 and Norm > 1.20). Excluding segments with $\chi^2/N > 2$ does not affect the normalizations of the included segments considerably. Similar conclusions were obtained by excluding the segments following the normalization criterion. Also, the data from Ref. [11] were fitted alone, starting

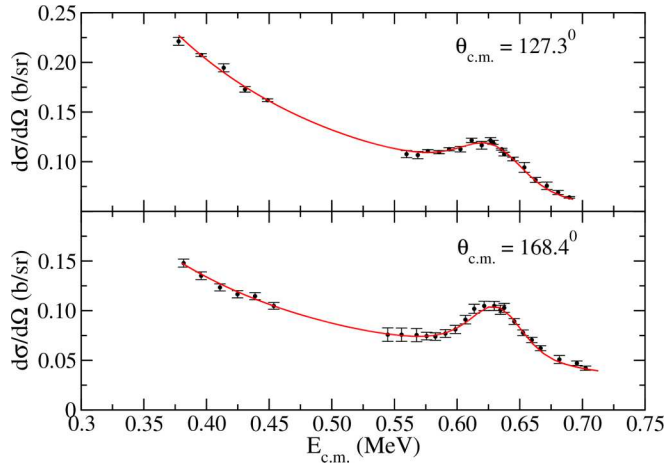

FIG. 12. ^{7}Be + p elastic scattering excitation function at low energies from Ref. [11]. The best fit is shown by the solid red curve, and filled black circles represent the data. The experimental cross section was convoluted to account for the 14- and 19-keV experimental resolutions reported in [11]. A systematic uncertainty of ±5.5% was included in the calculation.

TABLE III. *s*-wave scattering lengths for the ^{7}Be + *p* system.

a_{01} (fm)	a_{02} (fm)	Reference
$17.34^{+1.11}_{-1.33}$	$-3.18^{+0.55}_{-0.50}$	This work
25 ± 9	-7 ± 3	Angulo *et al.* [11]
-5.2	-15.3	Navratil *et al.* [12]

with the parameters in Table II, to evaluate the effects on the scattering length values. If the well-known states [2^+ (ground state), 1^+ (0.77 MeV), and 3^+ (3.52 MeV)] alone are included to fit the data from Ref. [11] along with the 2^- and 1^- background levels, we obtain *s*-wave scattering lengths consistent with the results in Ref. [11]. But with the introdution of the inelastic channel along with the inclusion of the 0^+ (1.9-MeV) and 2^+ (2.21-MeV) states, the results for the *s*-wave scattering lengths differ significantly from the results in Ref. [11]. The scattering lengths obtained from this analysis along with the values published in the literature are presented in Table III. Angulo *et al.* made the only previous determination of *s*-wave scattering lengths for the ^{7}Be + *p* system, where the cross-section data have been analyzed in an *R*-matrix framework and the *s*-wave scattering lengths have been deduced. Navratil *et al.* [12] used the *ab initio* no-core shell model/resonating group method to calculate the ^{7}Be$(p,\gamma)^8$B radiative capture cross section and deduce the *s*-wave scattering lengths for ^{7}Be + *p*. The *s*-wave scattering lengths from Ref. [12] do not agree with the results of this analysis.

In the context of the potential model [9], the extrapolation of S_{17} down to solar energies depends on the value of the average scattering length ($\bar{a}_0$), defined as

$$\bar{a}_0 = \frac{C^2_{(^3P_2)} a_{01} + C^2_{(^5P_2)} a_{02}}{C^2_{(^3P_2)} + C^2_{(^5P_2)}}. \quad (8)$$

The $\bar{a}_0$ value deduced in this work is $0.60^{+0.15}_{-0.18}$ fm using the ANC values from Ref. [32] neglecting their uncertainties. This shows that the average scattering length can be better constrained than the individual scattering lengths for channel spins 1 and 2, respectively.

V. CONCLUSIONS

The angular distributions for ^{7}Be + *p* elastic and inelastic scattering were measured in the center-of-mass energy range 0.474–2.740 MeV and center-of-mass angular range 70°–150°. Simultaneous fits of the angular distributions from this measurement and the excitation functions from Ref. [11] indicate the existence of a 0^+ state at 1.9 MeV and a 2^+ state at 2.21 MeV in ^{8}B. These states are required to explain the inelastic scattering excitation function, which shows a clear peak at 2.2 MeV. The results of this analysis do not provide conclusive evidence for the existence of a 1^+ level at 3.3 MeV in ^{8}B.

The experimental determination of *s*-wave scattering lengths for the ^{7}Be + *p* system from an *R*-matrix analysis of elastic and inelastic scattering data has been presented. The scattering length for channel spin 1 is in agreement with the previously reported scattering length in Ref. [11]. Our result for channel spin 2 lies just outside the 1σ lower limit of the scattering length reported in Ref. [11]. The general agreement between our results and those in Ref. [11] is not surprising, as the low-energy scattering data in Ref. [11] play a very significant role in both analyses. It can be inferred from Table III that the uncertainties in the *s*-wave scattering lengths have been reduced by a factor of 5–8 compared to the previous experimental measurement [11]. This lower uncertainty may reduce the overall uncertainty in $S_{17}(0)$, as discussed by Descouvemont [7] and Baye [9]. Using the potential model of Baye, the uncertainty in $S_{17}(0)$ due to the average scattering length $\bar{a}_0$ can be calculated using Eq. (20) from Ref. [9]. Using this approach, the uncertainty in the average scattering length $\bar{a}_0$ deduced in this work using Eq. (8) contributes the very small uncertainty of $\pm 0.03\%$ to $S_{17}(0)$, although it is not clear how this uncertainty impacts the extrapolation error on the $S_{17}(0)$ value deduced from capture data.

Besides this measurement, there is only one ^{7}Be + *p* elastic scattering measurement below 1 MeV. The measurements above this energy are not in agreement with each other. To better constrain the fits and the *R*-matrix parameters, more precise measurements are needed. Measurements below the 634-keV resonance are most important for constraining the scattering lengths. However, the data at higher energies are also important. Ideally, new scattering measurements would span a wide range of energy, from below the 634-keV resonance to well above 1 MeV. Transfer reactions could shed more light onto the structure of ^{8}B.

ACKNOWLEDGMENTS

We are grateful to R. J. deBoer for his assistance with AZURE2. We thank D. R. Phillips for taking part in constructive discussions. This work was supported in part by the U.S. Department of Energy under Grants No. DE-NA0002905, No. DE-NA0003883, No. DE-FG02-88ER40387, and No. DE-FG02-93ER40789 and Contract No. DE-AC05-00OR22725 (ORNL). D.W.B. acknowledges support from the NSF under Grant No. PHY-1713857. B.D. acknowledges support from the NSERC, Canada. The work of K.Y.C. was supported in part by National Research Foundation of Korea (NRF) Grants No. NRF-2016R1A5A1013277 and No. NRF-2013M7A1A1075764 funded by the Korean government (MEST). This research used resources of the Holifield Radioactive Ion Beam Facility, which was a DOE Office of Science User Facility operated by the Oak Ridge National Laboratory. The authors are grateful to the staff of the HRIBF whose hard work made the experiment possible.

[1] B. Aharmim *et al.* (SNO Collaboration), Phys. Rev. C **88**, 025501 (2013).

[2] K. Abe *et al.* (Super-Kamiokande Collaboration), Phys. Rev. D **94**, 052010 (2016).

[3] W. C. Haxton, R. G. Hamish Robertson, and A. M. Serenelli, Annu. Rev. Astron. Astrophys. **51**, 21 (2013).

[4] J. N. Bahcall, N. A. Bahcall, and R. K. Ulrich, Astrophys. J. **156**, 559 (1969).

[5] E. G. Adelberger, A. García, R. G. H. Robertson, K. A. Snover, A. B. Balantekin, K. Heeger, M. J. Ramsey-Musolf, D. Bemmerer, A. Junghans, C. A. Bertulani, J.-W. Chen, H. Costantini, P. Prati, M. Couder, E. Uberseder, M. Wiescher, R. Cyburt, B. Davids, S. J. Freedman, M. Gai, D. Gazit, L. Gialanella, G. Imbriani, U. Greife, M. Hass, W. C. Haxton, T. Itahashi, K. Kubodera, K. Langanke, D. Leitner, M. Leitner, P. Vetter, L. Winslow, L. E. Marcucci, T. Motobayashi, A. Mukhamedzhanov, R. E. Tribble, K. M. Nollett, F. M. Nunes, T.-S. Park, P. D. Parker, R. Schiavilla, E. C. Simpson, C. Spitaleri, F. Strieder, H.-P. Trautvetter, K. Suemmerer, and S. Typel, Rev. Mod. Phys. **83**, 195 (2011).

[6] C. R. Brune and B. Davids, Annu. Rev. Nucl. Part. Sci. **65**, 87 (2015).

[7] P. Descouvemont, Phys. Rev. C **70**, 065802 (2004).

[8] X. Zhang, K. M. Nollett, and D. R. Phillips, Phys. Rev. C **89**, 051602 (2014).

[9] D. Baye, Phys. Rev. C **62**, 065803 (2000).

[10] X. Zhang, K. M. Nollett, and D. Phillips, Phys. Lett. B **751**, 535 (2015).

[11] C. Angulo, M. Azzouz, P. Descouvemont, G. Tabacaru, D. Baye, M. Cogneau, M. Couder, T. Davinson, A. D. Pietro, P. Figuera, M. Gaelens, P. Leleux, M. Loiselet, A. Ninane, F. de Oliveira Santos, R. Pizzone, G. Ryckewaert, N. de Séréville, and F. Vanderbist, Nucl. Phys. A **716**, 211 (2003).

[12] P. Navratil, R. Roth, and S. Quaglioni, Phys. Lett. B **704**, 379 (2011).

[13] D. Tilley, J. Kelley, J. Godwin, D. Millener, J. Purcell, C. Sheu, and H. Weller, Nucl. Phys. A **745**, 155 (2004).

[14] V. Z. Gol'dberg, G. V. Rogachev, M. S. Golovkov, V. I. Dukhanov, I. N. Serikov, and V. A. Timofeev, J. Exp. Theor. Phys. Lett. **67**, 1013 (1998).

[15] G. V. Rogachev, J. J. Kolata, F. D. Becchetti, P. A. DeYoung, M. Hencheck, K. Helland, J. D. Hinnefeld, B. Hughey, P. L. Jolivette, L. M. Kiessel, H.-Y. Lee, M. Y. Lee, T. W. O'Donnell, G. F. Peaslee, D. Peterson, D. A. Roberts, P. Santi, and S. A. Shaheen, Phys. Rev. C **64**, 061601 (2001).

[16] H. Yamaguchi, Y. Wakabayashi, S. Kubono, G. Amadio, H. Fujikawa, T. Teranishi, A. Saito, J. He, S. Nishimura, Y. Togano, Y. Kwon, M. Niikura, N. Iwasa, K. Inafuku, and L. Khiem, Phys. Lett. B **672**, 230 (2009).

[17] J. P. Mitchell, G. V. Rogachev, E. D. Johnson, L. T. Baby, K. W. Kemper, A. M. Moro, P. Peplowski, A. S. Volya, and I. Wiedenhöver, Phys. Rev. C **87**, 054617 (2013).

[18] A. M. Lane and R. G. Thomas, Rev. Mod. Phys. **30**, 257 (1958).

[19] J. R. Beene, D. W. Bardayan, A. G. Uribarri, C. J. Gross, K. L. Jones, J. F. Liang, W. Nazarewicz, D. W. Stracener, B. A. Tatum, and R. L. Varner, J. Phys. G: Nucl. Part. Phys. **38**, 024002 (2011).

[20] R. P. Fitzgerald, Ph.D. dissertation, University of North Carolina, Chapel Hill, 2005.

[21] L. Gialanella, U. Greife, N. De Cesare, A. D'Onofrio, M. Romano, L. Campajola, A. Formicola, Z. Fulop, G. Gyürky, G. Imbriani, C. Lubritto, A. Ordine, V. Roca, D. Rogalla, C. Rolfs, M. Russo, C. Sabbarese, E. Somorjai, F. Strieder, F. Terrasi, and H. P. Trautvetter, Nucl. Instrum. Methods Phys. Res. Sec. B: Beam Interact. Mater. Atoms **197**, 150 (2002).

[22] D. W. Bardayan, J. C. Blackmon, C. R. Brune, A. E. Champagne, A. A. Chen, J. M. Cox, T. Davinson, V. Y. Hansper, M. A. Hofstee, B. A. Johnson, R. L. Kozub, Z. Ma, P. D. Parker, D. E. Pierce, M. T. Rabban, A. C. Shotter, M. S. Smith, K. B. Swartz, D. W. Visser, and P. J. Woods, Phys. Rev. C **62**, 055804 (2000).

[23] R. Livesay, Ph.D. dissertation, Colorado School of Mines, 2006.

[24] J. Ziegler and J. Biersack, Transport of ions in matter, TRIM program, version 95.06 (SRIM, 2003); https://www.srim.org.

[25] C. R. Brune and D. B. Sayre, Nucl. Instrum. Methods Phys. Res. Sec. A: Accelerat. Spectrom. Detect. Assoc. Equip. **698**, 49 (2013).

[26] J. E. Poling, E. Norbeck, and R. R. Carlson, Phys. Rev. C **13**, 648 (1976).

[27] P. Kunz, Finite range distorted wave Born approximation code, DWUCK5; http://spot.colorado.edu/~kunz/Home.html.

[28] J. E. Poling, E. Norbeck, and R. R. Carlson, Phys. Rev. C **5**, 1819 (1972).

[29] R. E. Azuma, E. Uberseder, E. C. Simpson, C. R. Brune, H. Costantini, R. J. de Boer, J. Görres, M. Heil, P. J. LeBlanc, C. Ugalde, and M. Wiescher, Phys. Rev. C **81**, 045805 (2010).

[30] C. R. Brune, Phys. Rev. C **66**, 044611 (2002).

[31] https://www.nndc.bnl.gov/ensdf.

[32] X. Zhang, K. M. Nollett, and D. R. Phillips, Phys. Rev. C **98**, 034616 (2018).

[33] K. M. Nollett and R. B. Wiringa, Phys. Rev. C **83**, 041001 (2011).

[34] D. Halderson, Phys. Rev. C **73**, 024612 (2006).

[35] H. A. Bethe, Phys. Rev. **76**, 38 (1949).

[36] J. Humblet, J. Math. Phys. **26**, 656 (1985).